Los Alamos NATIONAL LABORATORY EST.1943

LA-UR-15-22389 (Accepted Manuscript)

Sheath energy transmission in a collisional plasma with collisionless sheath

Tang, Xianzhu
Guo, Zehua

Provided by the author(s) and the Los Alamos National Laboratory (2018-06-18).

To be published in: Physics of Plasmas

DOI to publisher's version: 10.1063/1.4933415

Permalink to record: http://permalink.lanl.gov/object/view?what=info:lanl-repo/lareport/LA-UR-15-22389

Disclaimer:
Approved for public release. Los Alamos National Laboratory, an affirmative action/equal opportunity employer, is operated by the Los Alamos National Security, LLC for the National Nuclear Security Administration of the U.S. Department of Energy under contract DE-AC52-06NA25396. Los Alamos National Laboratory strongly supports academic freedom and a researcher's right to publish; as an institution, however, the Laboratory does not endorse the viewpoint of a publication or guarantee its technical correctness.

RESEARCH LIBRARY

Sheath energy transmission in a collisional plasma with collisionless sheath

Xian-Zhu Tang[1] and Zehua Guo[1]
Theoretical Division, Los Alamos National Laboratory, Los Alamos, NM 87545

(Dated: 7 October 2015)

Sheath energy transmission governs the plasma energy exhaust onto a material surface. The ion channel is dominated by convection, but the electron channel has a significant thermal conduction component, which is dominated by the Knudsen layer effect in the presence of an absorbing wall. First-principle kinetic simulations reveal a robustly supersonic sheath entry flow. The ion sheath energy transmission and the sheath potential are accurately predicted by a sheath model of truncated bi-Maxwellian electron distribution. The electron energy transmission is further enhanced by a parallel heat flux of the perpendicular degrees of freedom.

The plasma exhaust of particle and energy to a material surface is regulated by a non-neutral sheath that is on the order of plasma Debye length ($\lambda_{\rm de}$)[1]. This is generally known as the sheath boundary condition for plasma exhaust, which provides both a physical constraint for plasma sustainment[2–6] and a boundary condition for fluid (e.g.[7]) and reduced kinetic modeling (e.g.[8]) of a wall-bounded plasma. It has fundamental importance not only to laboratory plasmas in controlled fusion[1] and material processing[9], but also for space technology where man-made structures interact with the plasma environment[10,11].

In the canonical case where the plasma is either unmagnetized or has a magnetic field normal to the wall surface, the sheath boundary condition involves a sonic/supersonic flow at the sheath entrance which forms the boundary of the bulk quasi-neutral plasma. This comes about due to the well-known Bohm criterion in the standard sheath theory[12–15], which requires the outgoing flow at the sheath entrance $V_i^{se} = Mc_s \geq c_s$, with the sound speed c_s defined at the sheath entrance (labeled by superscript se) and Mach number $M \geq 1$. The ion particle flux to the wall is simply $\Gamma_i^{se} = n_i^{se} V_i^{se}$.

The plasma energy exhaust has both electron and ion channels, and these two energy transmission fluxes usually differ. They are set by the so-called sheath energy transmission coefficients, which are defined as the energy flux normalized by the particle exhaust flux times the temperature at the sheath entrance[1], $\gamma_e^{se} \equiv Q_e^{se}/\Gamma_e^{se} k_B T_e^{se}$, $\gamma_i^{se} \equiv Q_i^{se}/\Gamma_i^{se} k_B T_i^{se}$. The idea is that if $\gamma_{e,i}^{se}$ are intrinsic properties of the sheath, one can express the outgoing energy flux $Q_{e,i}^{se}$ in terms of the local plasma temperature ($T_{e,i}^{se}$) and density ($n_{e,i}^{se}$). Recalling that in the absence of an appreciable net current, $\Gamma_e^{se} = n_e^{se} V_e^{se} \approx Z\Gamma_i^{se} = Z n_i^{se} V_i^{se}$, one finds $V_e^{se} \approx V_i^{se}$ for the plasma being quasineutral at the sheath entrance $n_e^{se} \approx Z n_i^{se}$ (Z – ion charge).

The practical importance of sheath energy transmission can be illustrated by a hydrogen plasma in an infinite slab in which a source plasma is deposited at the center. The source plasma has an isotropic temperature $T^s = T_e^s = T_i^s$. In steady state, the ambipolar particle loss flux at the sheath entrance $\Gamma_i^{se} = \Gamma_e^{se} = \Gamma^{se}$ must be balanced by the deposition rate of the source plasma Γ_s, *i.e.*, $\Gamma_s = \Gamma^{se}$. The overall energy flux balance requires $\Gamma_s \left(\frac{3}{2}k_B T_e^s + \frac{3}{2}k_B T_i^s\right) = \gamma_i^{se}\Gamma^{se} k_B T_i^{se} + \gamma_e^{se}\Gamma^{se} k_B T_e^{se}$. In the limiting case of $T_e^{se} = T_i^{se} = T^{se}$, one finds that the sheath energy transmission coefficients directly set the plasma temperature at the sheath entrance in relation to the source temperature, $T^{se} = 3T^s/(\gamma_e^{se} + \gamma_i^{se})$.

In the case that a magnetic field intercepts the wall surface at an angle, the sheath theory is modified to take into account the gyromotion effect, which manifests in the so-called Chodura layer[16], in which a mostly field-aligned plasma ion exhaust flow obtains a significant transverse component toward the wall surface. As long as the angle is not too oblique, by which the gyro-orbit loss of ions can compete with the parallel loss of electrons, the conventional practice is to adapt the sheath boundary condition by geometrical projection at the sheath entrance[7], which in this case is just outside the Chodura layer. With this understanding, the focus here will be on $\gamma_{e,i}^{se}$ in the simpler case of normal magnetic incidence at the wall surface, a limiting case that also recovers the sheath energy transmission in an unmagnetized plasma.

This Letter reports first-principles kinetic simulation studies of $\gamma_{e,i}^{se}$ for fusion-relevant plasmas with mean-free-path $\lambda_{\rm mfp} >$ and $\gg \lambda_{\rm de}$, and comparable electron/ion temperatures. Our findings reveal significant difference on the sheath energy transmission, and to a lesser degree, sheath potential drop and ion exit speed at sheath entrance, in comparison with what are commonly used in fusion plasma modeling (e.g.[1,7]). These results are poised to impact the study of plasma-materials interaction, a topic of broad importance, and which is of particular urgency to magnetic fusion. The underlying physics will be elucidated in a theoretical formulation taking into account the plasma temperature anisotropy driven by sheath flow acceleration[17,18]. Namely a plasma with four separate temperatures ($T_{e\parallel}, T_{e\perp}, T_{i\parallel}, T_{i\perp}$) will be considered. In the absence of a magnetic field, $\parallel$ is with respect to the normal of the material surface instead of the magnetic field. Ignoring the perpendicular flow ($\mathbf{V}_\perp \approx 0$), one has the plasma species parallel energy flux

$$Q_\parallel = q_\parallel + \frac{1}{2} m V_\parallel^2 \Gamma_\parallel + \frac{3}{2} k_B T_\parallel \Gamma_\parallel + k_B T_\perp \Gamma_\parallel, \quad (1)$$

where $\mathbf{w} \equiv \mathbf{v} - \mathbf{V}$ and $q_\parallel = q_n/2 + q_s$ with

$$q_n \equiv \int m w_\parallel^3 f dv_\parallel d^2\mathbf{v}_\perp,\ q_s \equiv \int \frac{1}{2} m \mathbf{w}_\perp^2 w_\parallel f dv_\parallel d^2\mathbf{v}_\perp,$$

and $\frac{1}{2}k_BT_\parallel = \int \frac{1}{2}mw_\parallel^2 f dv_\parallel d^2\mathbf{v}_\perp$. The subtlety of the sheath energy transmission is entirely due to the thermal conduction flux $q_\parallel$. The root cause is that at the sheath entrance, the mean-free-path $\lambda_{\rm mfp}$ is typically much greater than the sheath width, which is on the order of Debye length, and thus the collisional closure for $q_\parallel$ would break down.

For the large ion-electron mass ratio, the ion heat flux is insignificant so γ_i^{se} is dominated by convection,

$$\gamma_i^{se} \equiv \frac{Q_{i\parallel}^{se}}{\Gamma_i^{se}k_BT_{i\parallel}^{se}} \approx \frac{1}{2}M^2\left(3+\frac{T_{e\parallel}^{se}}{T_{i\parallel}^{se}}\right)+\frac{3}{2}+\frac{T_{i\perp}^{se}}{T_{i\parallel}^{se}}, \quad (2)$$

where we have used the Bohm criterion $V_{i\parallel}^{se} = Mc_{s\parallel}$ with

$$c_{s\parallel} \equiv \sqrt{k_B(T_{e\parallel}^{se}+3T_{i\parallel}^{se})/m_i}. \quad (3)$$

Here we adopt an adiabatc index of 3 for ions, which is the one of a couple of conventional choices in the literature (e.g. Ref.[1,4]) that gives the highest sound speed. In the limiting case that $M = 1$ and $T_{e\parallel}^{se} = T_{i\parallel}^{se} = T_{i\perp}^{se}$, one has $\gamma_i^{se} = 4.5$. As we will see from the simulation data, the entry flow at the sheath entrance is consistently supersonic and $\gamma_i^{se} \sim 5.5$ is larger by order unity.

In contrast, electron sheath energy transmission has a significant thermal conduction component but negligible contribution from the convective flow energy flux,

$$\gamma_e^{se} \equiv \frac{Q_{e\parallel}^{se}}{\Gamma_e^{se}k_BT_{e\parallel}^{se}} \approx \frac{q_{e\parallel}^{se}}{\Gamma_{e\parallel}^{se}k_BT_{e\parallel}^{se}}+\frac{3}{2}+\frac{T_{e\perp}^{se}}{T_{e\parallel}^{se}}. \quad (4)$$

The dramatic impact of the Knudsen layer (namely the region within one $\lambda_{\rm mfp}$ from the wall) can be appreciated by estimating the heat transmission using a crude collisonal expression for $q_{e\parallel}$,

$$\frac{q_{e\parallel}^{se}}{\Gamma_{e\parallel}^{se}k_BT_{e\parallel}^{se}} = -\frac{\kappa_e}{n_e^{se}V_i^{se}}\frac{\nabla_\parallel T_{e\parallel}}{T_{e\parallel}} \sim \frac{\lambda_{\rm mfp}}{L_{T_e}}\sqrt{\frac{m_i}{m_e}}. \quad (5)$$

The Knudsen number $K_n = \lambda_{\rm mfp}/L_{T_e}$ is distinctly different depending on whether one looks upstream or downstream. In the upstream or away from the wall direction, L_{T_e} is the temperature gradient length scale, which is typically much longer than $\lambda_{\rm mfp}$ for a collisional plasma, predicting a heat flux typically less than $\Gamma_{e\parallel}^{se}k_BT_{e\parallel}^{se}$. In the downstream direction, the sheath entrance is only a few $\lambda_{\rm de}$ away from the wall, so L_{T_e} should be set to $\lambda_{\rm de}$. The so-called sheath Knudsen number $K_n^{sh} \equiv \lambda_{\rm mfp}/\lambda_{\rm de}$ is typically much greater than unity. This of course does not mean $q_{e\parallel}^{se} \gg \Gamma_{e\parallel}^{se}k_BT_{e\parallel}^{se}$ from Eq. (5), but simply indicates that the collisional closure breaks down in the Knudsen layer[19,20].

Our kinetic simulation is for a slab plasma with a source in the middle and absorbing walls at the ends. The plasma size is $L = 200\lambda_{\rm de}^s$, allowing an extended presheath region outside the source. The nominal Debye length $\lambda_{\rm de}^s \equiv \sqrt{T_e^s/m_e}/\omega_{pe}$ with ω_{pe} the plasma frequency, and the nominal mean-free-path $\lambda_{\rm mfp}^s \equiv \sqrt{2T_e^s/m_e}/\nu_{ee}$ with ν_{ee} the electron collision frequency, are defined using source plasma temperature and the initial plasma fill density. Once the source balancing the wall loss, the steady-state temperature and density are both lower, but give rise to a Debye length that is comparable. This setup is similar to that in Ref.[21] using the VPIC code[22], but now includes Coulomb collisions between same and different species. Maintaining $\lambda_{\rm mfp} \ll L$, we have scanned a range of nominal sheath Knudsen number $K_n^{sh} \equiv \lambda_{\rm mfp}^s/\lambda_{\rm de}^s$ from 5 to 166.7 corresponding to the local K_n^{sh} from ~ 1 to ~ 30. The mass ratio is fixed to be $m_i/m_e = 1600$, and source plasmas of isotropic temperature are deposited in the same rate as the ambipolar loss rate at the walls.

Figs. 1 and 2 show the sheath/presheath structure for a highly collisional plasma ($K_n^{sh} = 5$) versus one having an approximately collisionless sheath ($K_n^{sh} = 50$). Using the breakdown of quasi-neutrality as a criterion (1% charge density separation, as dictated by the noise level in PIC simulations with 40000 particles per cell), one finds that the sheath entrance is approximately at $x = 196\lambda_{\rm de}^s$, about 4 $\lambda_{\rm de}^s$ away from the wall. In the plots, the densities are normalized against the initial fill plasma density n_0, temperature the source plasma temperature T_s, and flow $\sqrt{T_s/m_e}$. With strong collisionality, the electron and ion temperatures are approximately isotropic, despite a large deviation from the source temperature, Fig. 1. With $K_n^{sh} \gg 1$, the electron develops strong temperature anisotropy in the sheath and the Knudsen layer part of the presheath, in addition to significant T_e-T_i separation, Fig. 2. The large ion temperature anisotropy is due to the much slower collisional isotropization rate and strong parallel cooling of initially isotropic source ions. Surprisingly $T_{e\perp}$ can spike up near the wall especially for lower collisionality. This can be the result of pitch angle scattering by the whistler waves driven by the trapped electrons[21]. Since PIC simulations do not have the resolution to resolve the low amplitude waves that are likely localized to the wall region, a clear resolution remains a future work.

An interesting and important result from Figs. 1 and 2 concerns the Bohm criterion in a warm ion plasma. At the sheath entrance, the ion flow is observed to be robustly supersonic with sound speed defined in Eq. (3). Although this is less a surprise for a highly collisional plasma[23–25], the fact that $M = 1.08$ even for the $K_n^{sh} = 166.7$ case can be a concern. This observation in warm-ion plasma appears to be consistent with a previous cold-ion collisionless simulation[26] that found $M = 1.19$ at sheath entrance, notwithstanding the long-held belief of a sonic transition and prior simulations that support it (e.g. [27]). Having a supersonic as opposed to sonic transition at the sheath entrance so-defined can impact the evaluation of sheath potential drop and as we shall show, the sheath energy transmission.

The plasma state at the sheath entrance is characterized by four dimensionless parameters: $M \equiv$

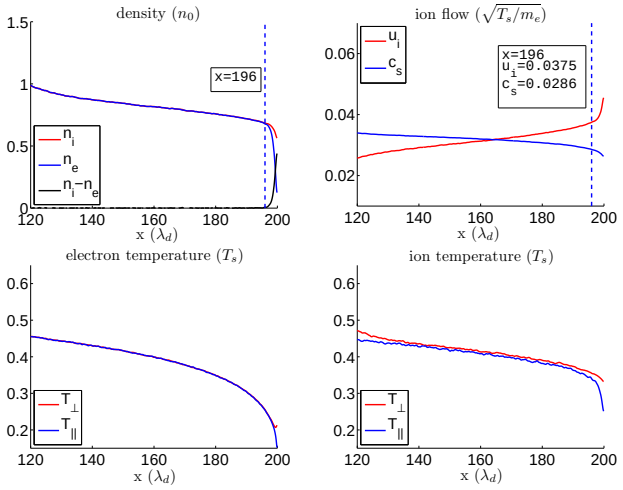

FIG. 1. For a very collisional plasma with nominal $\lambda^s_{\rm mfp}/\lambda^s_{\rm de} = 5$, there is little temperature anisotropy and T_e-T_i separation. The ion flow at the sheath entrance is supersonic using sound speed definition in Eq. (3).

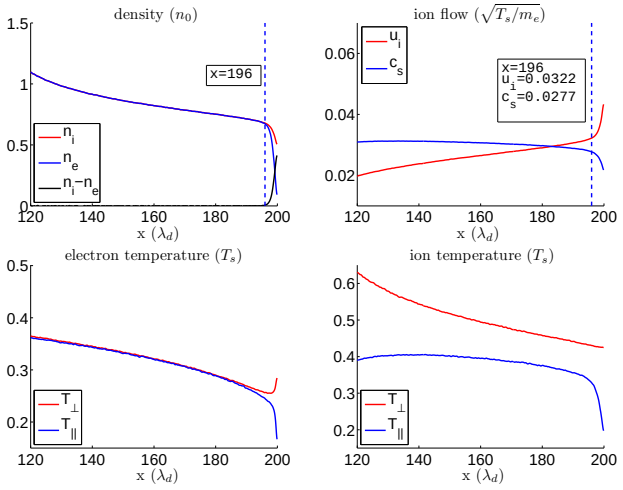

FIG. 2. With less collisionality (nominal $\lambda^s_{\rm mfp}/\lambda^s_{\rm de} = 50$), electron temperature anisotropy develops in the sheath and the Knudsen layer part of the presheath. The ion flow remains supersonic at sheath entrance.

$V^{se}_{i\parallel}/c^{se}_{s\parallel}, T^{se}_{i\parallel}/T^{se}_{e\parallel}, T^{se}_{e\perp}/T^{se}_{e\parallel}$ and $T^{se}_{i\perp}/T^{se}_{i\parallel}$. The simulation results of these are tabulated in Table I, along with the observed ion and electron sheath energy transmission coefficients, and the normalized sheath potential drop. The ion sheath energy transmission only has a small scatter around 5.5 which is greater by one than γ^{se}_i from the limiting case of $M = 1$ and $T^{se}_{e\parallel} = T^{se}_{i\parallel} = T^{se}_{i\perp}$, as noted earlier. It must be noted that for varying collisionality, there is a significant trade-off between M and $T^{se}_{i\perp}/T^{se}_{i\parallel}$ to achieve a similar value of γ^{se}_i. When using the $M, T^{se}_{i\parallel}/T^{se}_{e\parallel}, T^{se}_{i\perp}/T_{i\parallel}$ data from the simulation, Eq. (2) shows excellent agreement with the simulation. This can be seen by contrasting the γ^{se}_i column in Table I with

$\frac{\lambda_{\rm mfp}}{\lambda_{\rm de}}$	M	$\frac{T^{se}_{i\parallel}}{T^{se}_{e\parallel}}$	$\frac{T^{se}_{i\perp}}{T^{se}_{i\parallel}}$	$\frac{T^{se}_{e\perp}}{T^{se}_{e\parallel}}$	$\frac{e\Delta\Phi^{sh}}{k_B T^{se}_{e\parallel}}$	γ^{se}_i	γ^{se}_e	$\gamma^{se(-)}_e$	α
5	1.31	1.34	1.04	1.00	-1.82	5.86	3.86	3.33	0.64
16.7	1.23	1.38	1.09	1.01	-2.02	5.60	4.24	3.58	0.61
50	1.16	1.35	1.31	1.05	-2.16	5.42	4.85	4.22	0.38
166.7	1.08	1.18	2.03	1.09	-2.30	5.95	5.27	4.70	0.27

TABLE I. Simulation results for $m_i/m_e = 1600$. Here $\alpha \equiv 2q^{se}_{e,s}/q^{se}_{e,n}$ and $\gamma^{se(-)}_e \equiv \gamma^{se}_e - q^{se}_{e,s}/\Gamma^{se}_{e\parallel} k_B T^{se}_{e\parallel}$. The γ^{se}_e and γ^{se}_i are computed from the simulated $Q^{se}_\parallel$ and $\Gamma_\parallel T^{se}_\parallel$.

that in Table II. The remaining discrepancy is due to the small parallel ion heat flux.

The simulation results in Table I also reveals (1) a sheath potential drop that is in the neighborhood of $2T^{se}_{e\parallel}$; and (2) substantial variation in the electron energy transmission coefficient. Fortunately, the first-principle kinetic simulations show some salient features in the electron distribution function that are anticipated by intuitive physics arguments. This enables a simple model analysis to help elucidate the physics behind the observed $e\Delta\Phi^{sh}/k_B T^{se}_{e\parallel}$ and γ^{se}_e.

$\frac{\lambda_{mfp}}{\lambda_{\rm de}}$	$\Delta\varphi^{sh}$	$\frac{T^{se}_{e\parallel}}{T^0_{e\parallel}}$	$\frac{e\Delta\Phi^{sh}}{k_B T^{se}_{e\parallel}}$	γ^{se}_i	γ^{se}_e
5	-1.79	0.87	-2.07	5.75	4.23
16.7	-1.84	0.87	-2.11	5.41	4.27
50	-1.90	0.88	-2.17	5.33	4.36
166.7	-2.02	0.89	-2.27	5.77	4.49

TABLE II. Model preditions for $m_i/m_e = 1600$. The four dimensionless input parameters of the model, $M, T^{se}_{i\parallel}/T^{se}_{e\parallel}, T^{se}_{i\perp}/T^{se}_{i\parallel}$, and $T^{se}_{e\perp}/T^{se}_{e\parallel}$, are taken from the similaution data tabluated in Table I.

For a plasma with $L \gg \lambda_{\rm mfp} \gg \lambda_{\rm de}$, the electron outside the Knudsen layer is collisionally relaxed to approximately a local Maxwellian. Once inside the Knudsen layer and certainly the sheath, the electrons become collisionless. The Vlasov solution in this region is a function of the invariants of motion. Ignoring the drift motion, the electrons have two constants of motion: the magnetic moment $\mu \equiv m_e v^2_\perp/2B$, and the total energy $\mathcal{E} = \frac{1}{2}m_e v^2_\parallel + \mu B - e\Phi(x)$. In the simpler case of a uniform magnetic field (i.e. small magnetic field variation on Debye length scale), μB is also a constant of motion, so is the parallel energy $\frac{1}{2}m_e v^2_\parallel - e\Phi(x)$. As the result, the following truncated double Maxwellian is a Vlasov solution that can be expected from the local Maxwellian further upstream,

$$f_e = n^0_e \sqrt{\frac{m_e}{2\pi k_B T^0_{e\parallel}}} \exp\left(-\frac{\frac{1}{2}m_e v^2_\parallel - e\Phi(x)}{k_B T^0_{e\parallel}}\right) \frac{m_e}{2\pi k_B T^0_{e\perp}} \exp\left(-\frac{\frac{1}{2}m_e v^2_\perp}{k_B T^0_{e\perp}}\right). \quad (6)$$

Here $n_e^0, T_{e\|}^0$ and $T_{e\perp}^0$ are all constants to be specified in terms of plasma density and temperatures at the sheath entrance. The truncation in $v_\|$ for electrons moving away from the wall, namely $f_e = 0$ for $v_\| < -v_c$ with $v_c(x) \equiv \sqrt{-2e\left[\Phi(x_w) - \Phi(x)\right]/m_e}$, is simply the result of wall absorption of electrons with kinetic energy greater than the potential hill between the current location (x) of the electron and the wall (x_w). At the sheath entrance ($x = x_s$), the sheath potential drop $\Delta\Phi^{sh} \equiv \Phi(x = x_w) - \Phi(x_s)$, so $v_c^{se} \equiv \sqrt{-2e\Delta\Phi^{sh}/m_e}$.

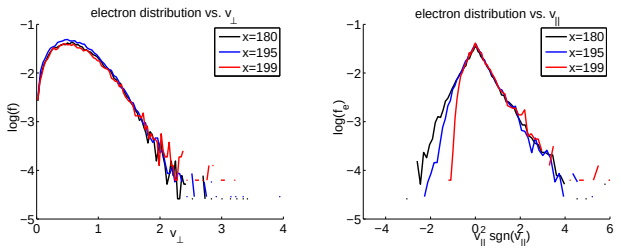

FIG. 3. The electron distribution function at three locations. The local $\lambda_{\rm mfp}/\lambda_{\rm de}$ are approximately $25 - 30$.

In Fig. 3 the electron distribution at different locations clearly show the transition from a local Maxwellian to a truncated bi-Maxwellian from our kinetic simulations. This provides direct support for the truncated Maxwellian for electrons in sheath modeling[19,20], though with anisotropic temperatures. The detailed transition is a complicated process, but having the form of the truncated bi-Maxwellian distribution is sufficient to construct the sheath model for evaluating both the sheath potential drop and the energy transmission.

To do that, one takes velocity moments of the distribution and solves $n_e^0, T_{e\|}^0$, and $T_{e\perp}^0$, in terms of $n_e^{se}, T_{e\|}^{se}$, and $T_{e\perp}^{se}$. The zeroth and first order moments give

$$n_e^{se} = (n_e^0/2)\exp\left[\varphi(x_s)\right]\left[1 + \mathrm{Erf}\left(\sqrt{-\Delta\varphi^{sh}}\right)\right], \quad (7)$$

$$\Gamma_{e\|}^{se} = \int_{-v_c^{se}}^{\infty} f_e(x_s) v_\| dv_\| d^2\mathbf{v}_\perp = \frac{n_e^0}{2} e^{\varphi(0)} v_{th,e}^0. \quad (8)$$

with $\varphi(x) \equiv e\Phi(x)/k_B T_{e\|}^0$ and $v_{th,e}^0 \equiv \sqrt{2k_B T_{e\|}^0/\pi m_e}$. The electron particle flux can be rewritten in terms of n_e^{se} given in Eq. (7), $\Gamma_{e\|}^{se} = n_e^{se} V_{e\|}^{se}$ with $V_{e\|}^{se} = \exp\left[\Delta\varphi^{sh}\right]\left[1 + \mathrm{Erf}\left(\sqrt{-\Delta\varphi^{sh}}\right)\right]^{-1} v_{th,e}^0$ the electron flow at the sheath entrance. Noting that the last factor is the electron thermal speed, so the Boltzman factor needs to be small to bring the speed down to ion sound speed level due to the requirement of ambipolarity, $\Gamma_e^{se} = Z\Gamma_i^{se}$, which, written out explicitly, is

$$Mc_{s\|} = \exp\left[\Delta\varphi^{sh}\right]\left[1 + \mathrm{Erf}\left(\sqrt{-\Delta\varphi^{sh}}\right)\right]^{-1} v_{th,e}^0. \quad (9)$$

Integrating the second moment of the truncated distribution function, one finds that $T_{e\perp}^{se} = T_{e\perp}^0$ and

$$\frac{T_{e\|}^{se}}{T_{e\|}^0} = 1 - \frac{\frac{2}{\sqrt{\pi}}\sqrt{-\Delta\varphi^{sh}}e^{\Delta\varphi^{sh}}}{1 + \mathrm{Erf}\left(\sqrt{-\Delta\varphi^{sh}}\right)} - \frac{\frac{2}{\pi}e^{2\Delta\varphi^{sh}}}{\left[1 + \mathrm{Erf}\left(\sqrt{-\Delta\varphi^{sh}}\right)\right]^2} \quad (10)$$

The coupled Eq. (9) and Eq. (10) can be solved for $\Delta\Phi^{sh}$ and $T_{e\|}^0$ in terms of $T_{e\|}^{se}$, with $T_{i\|}^{se}/T_{e\|}^{se}$ an independent input parameter in the sheath model. Using $T_{i\|}^{se}/T_{e\|}^{se}$ from the kinetic simulation, we find the model prediction of $e\Delta\Phi^{sh}/k_B T_{e\|}^{se}$ (Table II) is in excellent agreement with direct simulation (Table I) in the $K_n^{sh} \gg 1$ regime.

The model prediction of the electron parallel heat flux with the Vlasov solution in Eq. (6) has an intrinsic defect in that $q_{e,s} = 0$. The $q_{e,n}$ component with the truncated bi-Maxwellian is,

$$\frac{q_{e,n}^{se}}{\Gamma_{e\|}^{se} k_B T_{e\|}^{se}} = -\frac{e\Delta\Phi^{sh}}{k_B T_{e\|}^{se}} + \left(\frac{T_{e\|}^0}{T_{e\|}^{se}} - \frac{3}{2}\right) + O\left(\frac{m_e}{m_i}\right). \quad (11)$$

The electron sheath energy transmission coefficient predicted by the truncated bi-Maxwellian model is

$$\gamma_e^{se} \equiv \frac{Q_{e\|}^{se}}{\Gamma_{e\|}^{se} k_B T_{e\|}^{se}} = -\frac{e\Delta\Phi^{sh}}{k_B T_{e\|}^{se}} + \frac{T_{e\|}^0}{T_{e\|}^{se}} + \frac{T_{e\perp}^{se}}{T_{e\|}^{se}}. \quad (12)$$

Table II tabulates the model prediction of γ_e^{se} based on the simulated plasma parameters at the sheath entrance. Since $q_{e,s} = 0$ for the truncated bi-Maxwellian model, one anticipates an under-prediction compared with the kinetic simulation for $K_n^{sh} \gg 1$, which is indeed the case by contrasting Table II and I. If we remove the $q_{e,s}$ contribution to $q_{e\|}^{se}$ in the simulation data by computing $\gamma_e^{se(-)} \equiv \gamma_e^{se} - q_{e,s}^{se}/\Gamma_{e\|}^{se} k_B T_{e\|}^{se}$, one finds the interesting trend that with decreasing collisionality, the truncated bi-Maxwellian model transitions from over-predict to under-predict the $q_{e,n}^{se}$. Also of interest is the ratio of $q_{e,s}/q_{e,n}$, which decreases as K_n^{sh} increases. Previously we have found that $q_{e,s}/q_{e,n}$, however, does not vanish in the limit of $K_n^{sh} \to \infty$. This is due to the excitation of trapped electron Whistler wave, which through wave-particle interactions, drives a finite $q_{e,s}$ in the absence of Coulomb collisions[21].

Introducing $\alpha \equiv 2q_{e,s}^{se}/q_{e,n}^{se}$, one can parameterize the model prediction of γ_e^{se} as

$$\begin{aligned}\gamma_e^{se} &= (1+\alpha)\frac{q_{e,n}^{se}}{\Gamma_{e\|}^{se} k_B T_{e\|}^{se}} + \frac{3}{2} + \frac{T_{e\perp}^{se}}{T_{e\|}^{se}} \\ &= (1+\alpha)\left(-\frac{e\Delta\Phi^{sh}}{k_B T_{e\|}^{se}} + \frac{T_{e\|}^0}{T_{e\|}^{se}} - \frac{3}{2}\right) + \frac{3}{2} + \frac{T_{e\perp}^{se}}{T_{e\|}^{se}}.\end{aligned} \quad (13)$$

The sheath potential drop, which can be calculated accurately in the model, plays a critical role in sheath energy transmission in addition to the subtlety of $q_{e,s}/q_{e,n}$.

In conclusion, kinetic simulations of a warm-ion plasma show a persistent supersonic exit flow at the sheath entrance (defined as the location where electron and ion charge density deviates by 1%), with a sound speed defined in Eq. (3). The sheath potential drop can be accurately determined by solving Eqs. (9,10), yielding a potential drop that can deviate appreciably, especially for high collisionality, from the usual practice that deploys a sonic transition and ignores the temperature correction due to truncated electron distribution, namely by setting $M = 1$ and $\mathrm{Erf}\left(\sqrt{-\Delta\varphi^{sh}}\right) = 0$ in Eq. (9), and $T^{se}_{e\|} = T^{0}_{e\|}$ in lieu of Eq. (10). The ion sheath energy transmission, dominated by convection, is accurately given by Eq. (2). Four dimensionless parameters, Mach number, mass ratio, electron-ion parallel temperature ratio, and electron temperature anisotropy, enter explicitly into the electron sheath energy transmission, which has a substantial contribution from thermal conduction $q^{se}_{e,n}$, mostly due to loss of high-energy electrons to an absorbing wall. The parallel thermal conduction flux of the perpendicular degrees of freedom, $q^{se}_{e,s}$, can make a sizeable contribution to electron sheath energy transmission, and physically it is the result of correlations between parallel and perpendicular fluctuations, for which the physics of wave excitation, wave-particle interaction, and Coulomb collisions must be resolved.

This work was funded by the U.S. Department of Energy Office of Science, Office of Fusion Energy Sciences and Advanced Scientific Computing Research, under the auspices of the National Nuclear Security Administration of the U.S. Department of Energy by Los Alamos National Laboratory, operated by Los Alamos National Security LLC under contract DE-AC52-06NA25396.

[1] P. C. Stangeby, *The Plasma Boundary of Magnetic Fusion Devices* (Taylor & Francis, 2000).
[2] G. D. Hobbs and J. A. Wesson, Plasma Physics **9**, 85 (1967).
[3] H. Kimura, H. Maeda, N. Ueda, M. Seki, H. Kawamura, S. Yamamoto, M. Nagami, K. Odajima, S. Sengoku, and Y. Shimomura, Nuclear Fusion **18**, 9 (1978).
[4] R. C. Bissell, P. C. Johnson, and P. C. Stangeby, Phys. Fluids B **1**, 1133 (1989).
[5] S. Jachmich, T. Eich, W. Fundamenski, A. Kallenbach, R. A. Pitts, and J.-E. Contributros, Journal of Nuclear Materials **363-365**, 1050 (2007).
[6] S. Marsen, T. Eich, M. Groth, S. Jachmich, and B. Sieglin, Journal of Nuclear Materials **438**, S393 (2013).
[7] R. Schneider, X. Bonnin, K. Borrass, D. P. Coster, H. Kastelewicz, D. Reiter, V. A. Rozhansky, and B. J. Braams, Contrib. Plasma Phys. **46**, 3 (2006).
[8] C. S. Chang, S. Klasky, J. Cummings, R. Samtaney, A. Shoshani, L. Sugiyama, D. Keyes, S. Ku, G. Park, S. Parker, N. Podhorszki, H. Strauss, H. Abbasi, M. Adams, R. Barreto, G. Bateman, K. Bennett, Y. Chen, E. D. Azevedo, C. Docan, S. Ethier, E. Feibush, L. Greengard, T. Hahm, F. Hinton, C. Jin, A. Khan, A. Kritz, P. Krsti, T. Lao, W. Lee, Z. Lin, J. Lofstead, P. Mouallem, M. Nagappan, A. Pankin, M. Parashar, M. Pindzola, C. Reinhold, D. Schultz, K. Schwan, D. Silver, A. Sim, D. Stotler, M. Vouk, M. Wolf, H. Weitzner, P. Worley, Y. Xiao, E. Yoon, and D. Zorin, in *SCIDAC 2008: SCIENTIFIC DISCOVERY THROUGH ADVANCED COMPUTING*, Journal of Physics Conference Series, Vol. 125, edited by Stevens, RL (US DOE Off Sci; Cray; IBM; Intel; HP; SiCortex, 2008) p. 12042, 4th Annual Scientific Discovery through Advanced Computing Conference (SciDAC 2008), Seattle, WA, JUL 13-17, 2008.
[9] M. A. Lieberman and A. J. Lichtenberg, *Principles of Plasma Discharges and Materials Processing*, 2nd ed. (Wiley-Interscience, 2005).
[10] D. E. Hastings and H. B. Garrett, *Spacecraft-Environment Interactions* (Cambridge University Press, Cambridge, UK, 1996).
[11] S. T. Lai, *Fundamentals of Spacecraft Charging: Spacecraft Interactions with Space Plasmas* (Princeton University Press, Princeton, NJ, 2011).
[12] D. Bohm, *The Characteristics of Electrical Discharges in Magnetic Fields* (Mc-Graw-Hill, New York, 1949).
[13] K. U. Riemann, Journal of Physics D - Applied Physics **24**, 493 (1991).
[14] S. D. Baalrud and C. C. Hegna, Plasma Sources Science & Technology **20**, 025013 (2011).
[15] S. D. Baalrud, B. Scheiner, B. Yee, M. Hopkins, and E. Barnat, Plasma Phys. Control. Fusion **57**, 044003 (2015).
[16] R. Chodura, Phys. Fluids **25**, 1628 (1982).
[17] X.-Z. Tang, Plasma Physics and Controlled Fusion **53**, 082002 (2011).
[18] Z. Guo, X.-Z. Tang, and C. McDevitt, Physics of Plasmas **21**, 102512 (2014).
[19] G. A. Emmert, R. M. Wieland, A. T. Mense, and J. N. Davidson, Phys. Fluids **23**, 803 (1980).
[20] R. Marchand, Z. Abou-Assaleh, and J. P. Matte, Physics of Fluids B **2**, 1247 (1990).
[21] Z. Guo and X.-Z. Tang, Phys. Rev. Lett. **109**, 135005 (2012).
[22] K. Bowers, B. Albright, L. Yin, B. Bergen, and T. Kwan, Physics of Plasmas **15**, 055703 (2008).
[23] J. INGOLD, PHYSICS OF FLUIDS **15**, 75 (1972).
[24] A. METZE, D. ERNIE, and H. OSKAM, PHYSICAL REVIEW A **39**, 4117 (1989).
[25] E. ZAWAIDEH, N. KIM, and F. NAJMABADI, PHYSICS OF FLUIDS B-PLASMA PHYSICS **2**, 647 (1990).
[26] J. Sheehan, H. N., I. Kaganovich, H. Wang, Y. Raitses, E. Barnat, W. B.R., and S. D., Phys. Rev. Lett. **111**, 075002 (2013).
[27] J. T. Gudmundsson and M. A. Lieberman, PHYSICAL REVIEW LETTERS **107** (2011), 10.1103/PhysRevLett.107.045002.

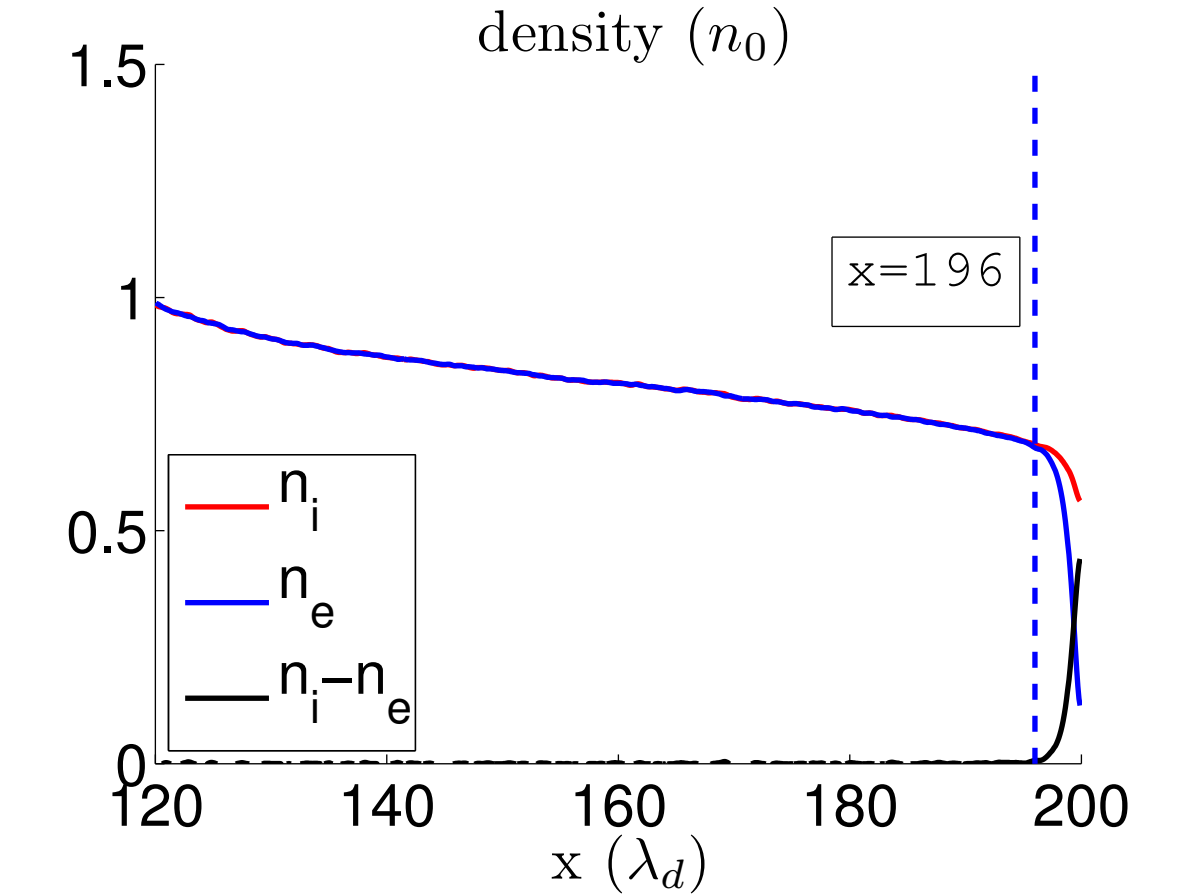
density (n_0)
1.5
1
0.5
0
120
140
160
180
200
x (λ_d)
x=196
n_i
n_e
n_i–n_e

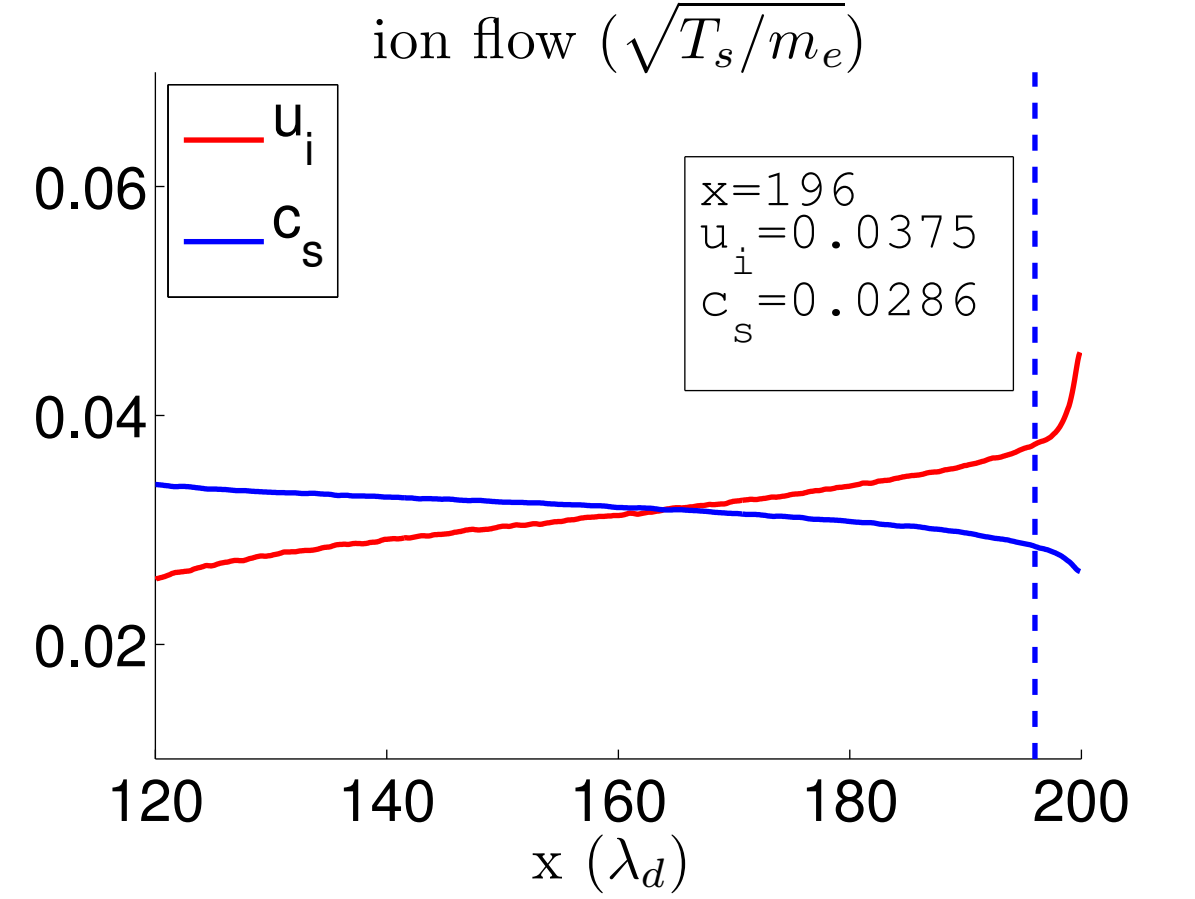
ion flow ($\sqrt{T_s/m_e}$)
u_i
c_s
x=196
u_i=0.0375
c_s=0.0286
0.06
0.04
0.02
120
140
160
180
200
x (λ_d)

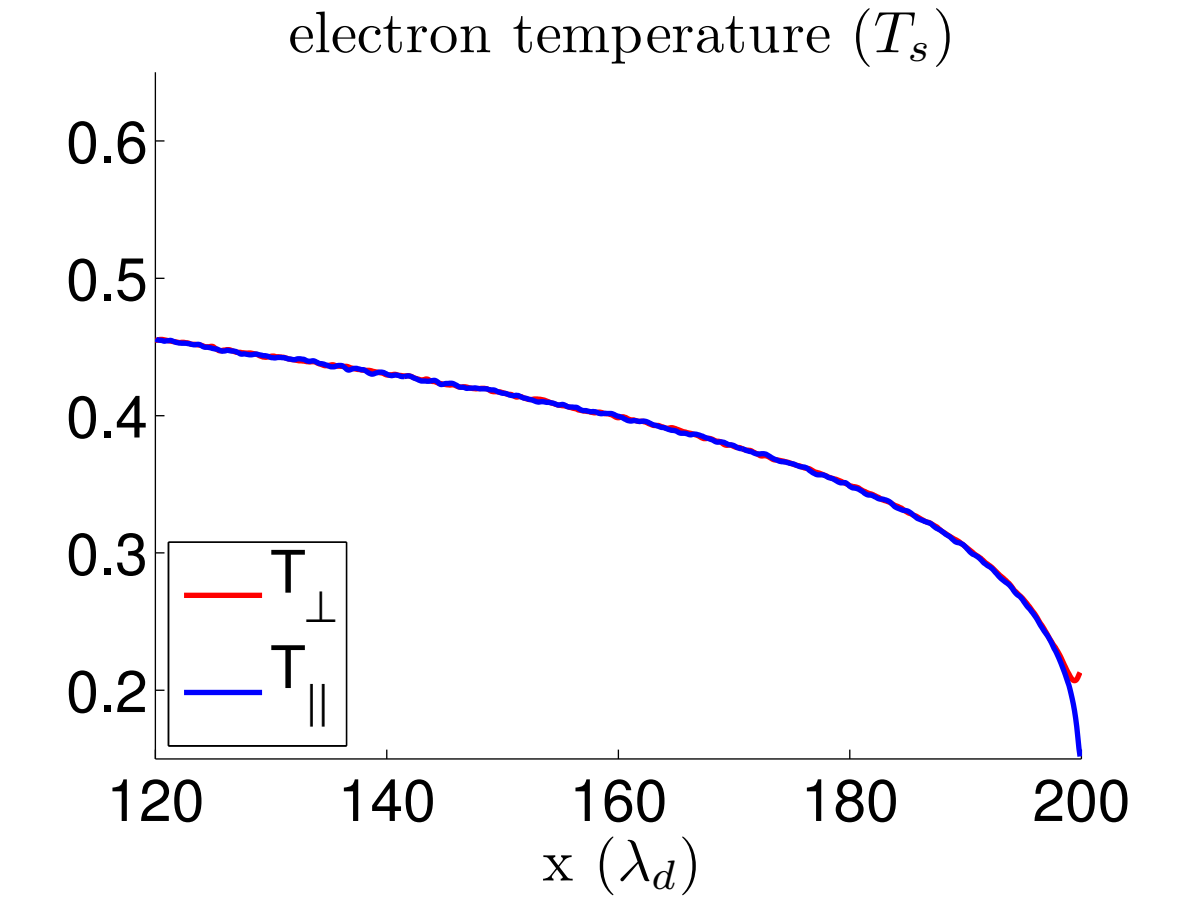
electron temperature (T_s)
0.6
0.5
0.4
0.3
0.2
$T_\perp$
$T_{||}$
120
140
160
180
200
x (λ_d)

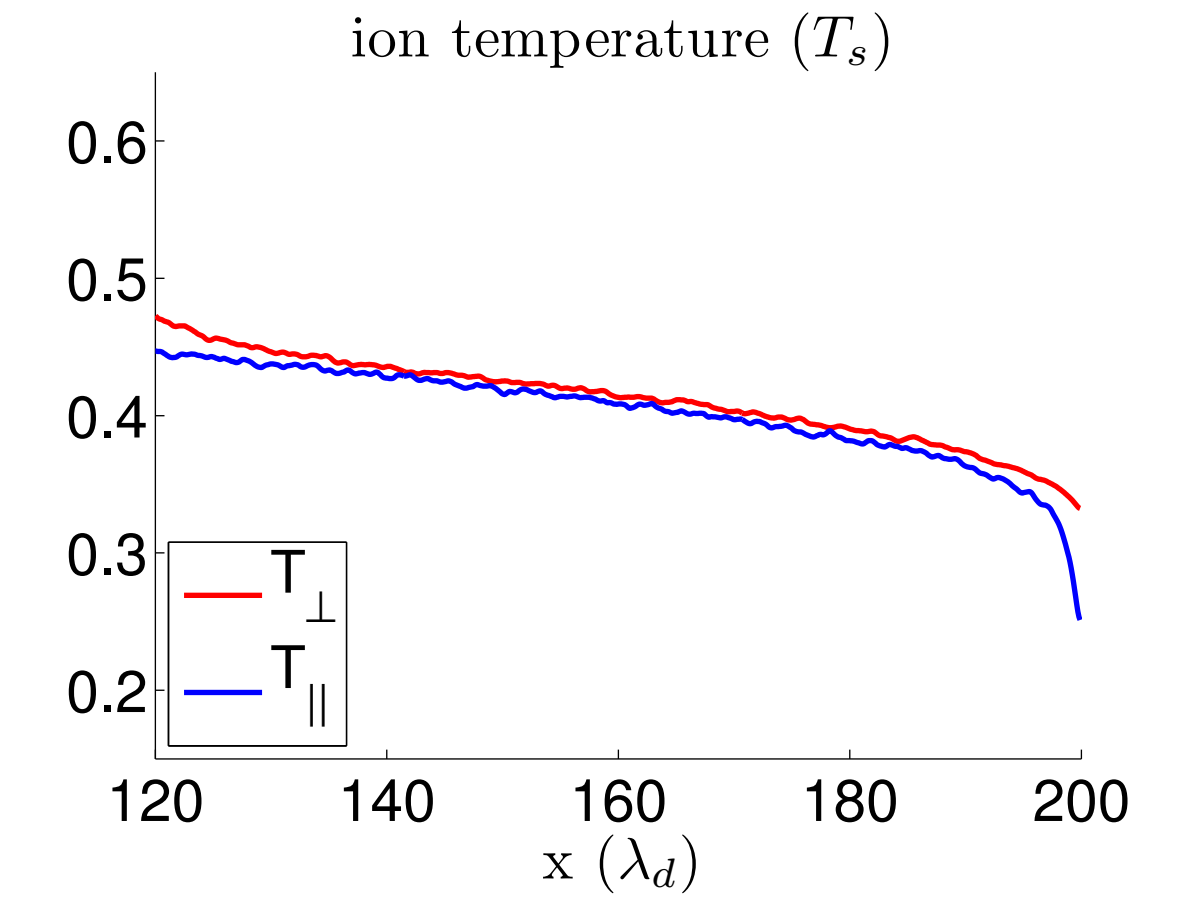
ion temperature (T_s)
0.6
0.5
0.4
0.3
0.2
$T_\perp$
$T_{||}$
120
140
160
180
200
x (λ_d)

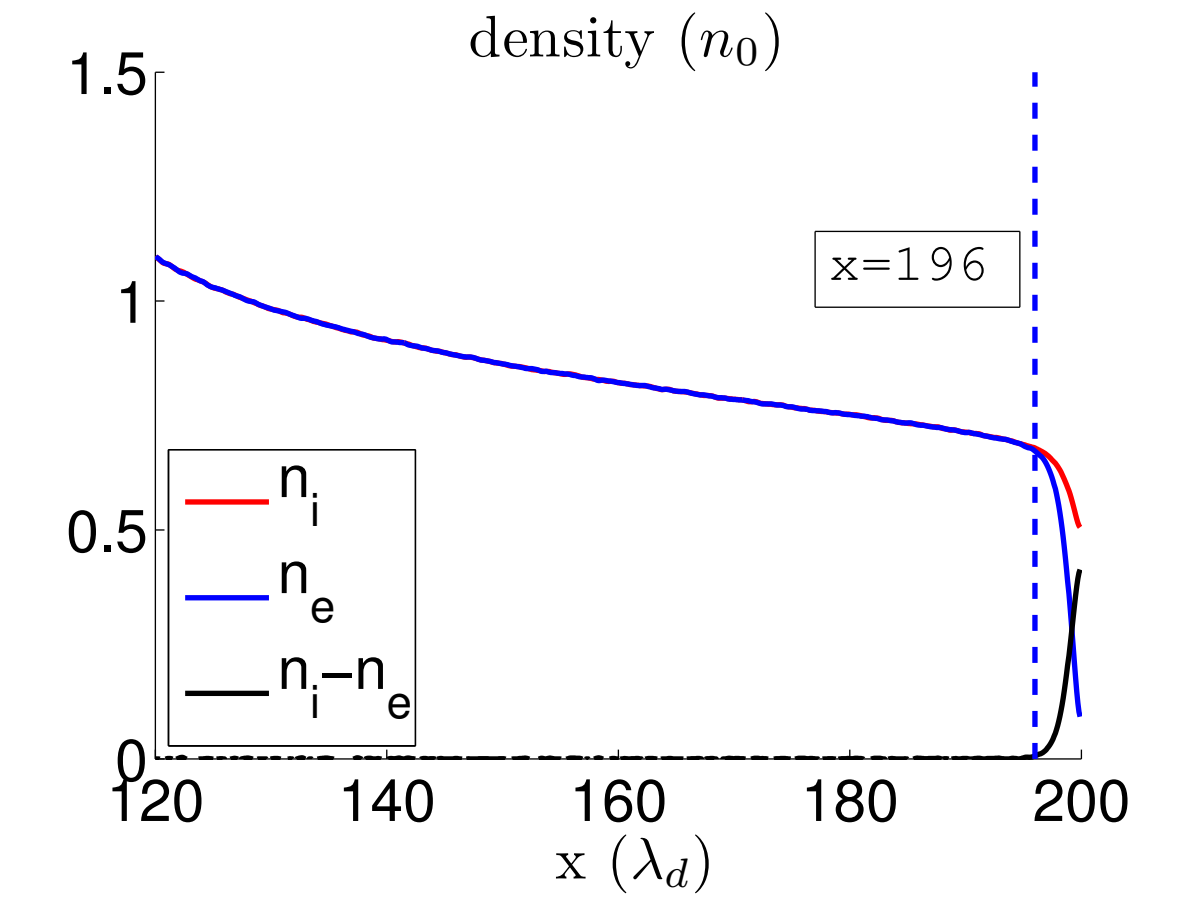
density (n_0)
1.5
1
0.5
0
120
140
160
180
200
x (λ_d)
x=196
n_i
n_e
n_i–n_e

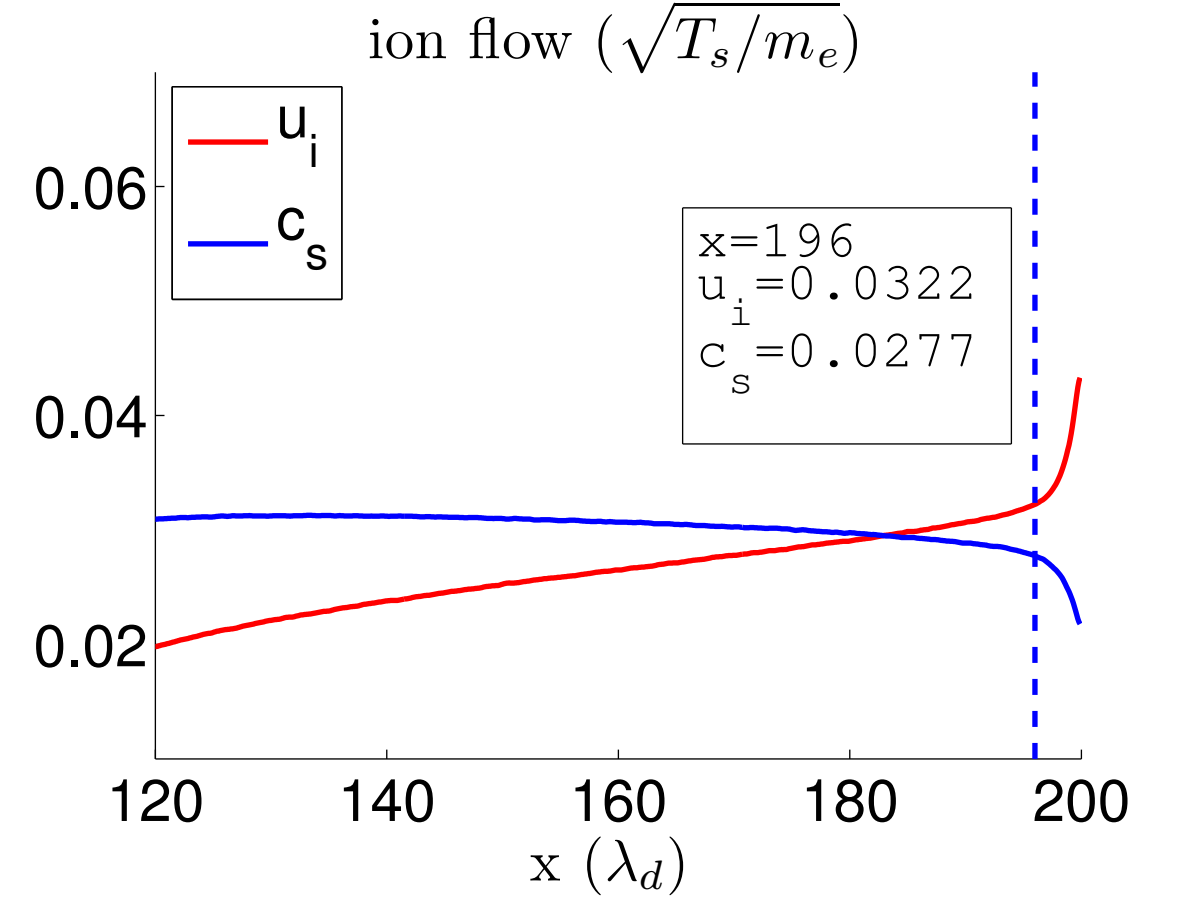
ion flow ($\sqrt{T_s/m_e}$)
u_i
c_s
x=196
u_i=0.0322
c_s=0.0277
0.06
0.04
0.02
120
140
160
180
200
x (λ_d)

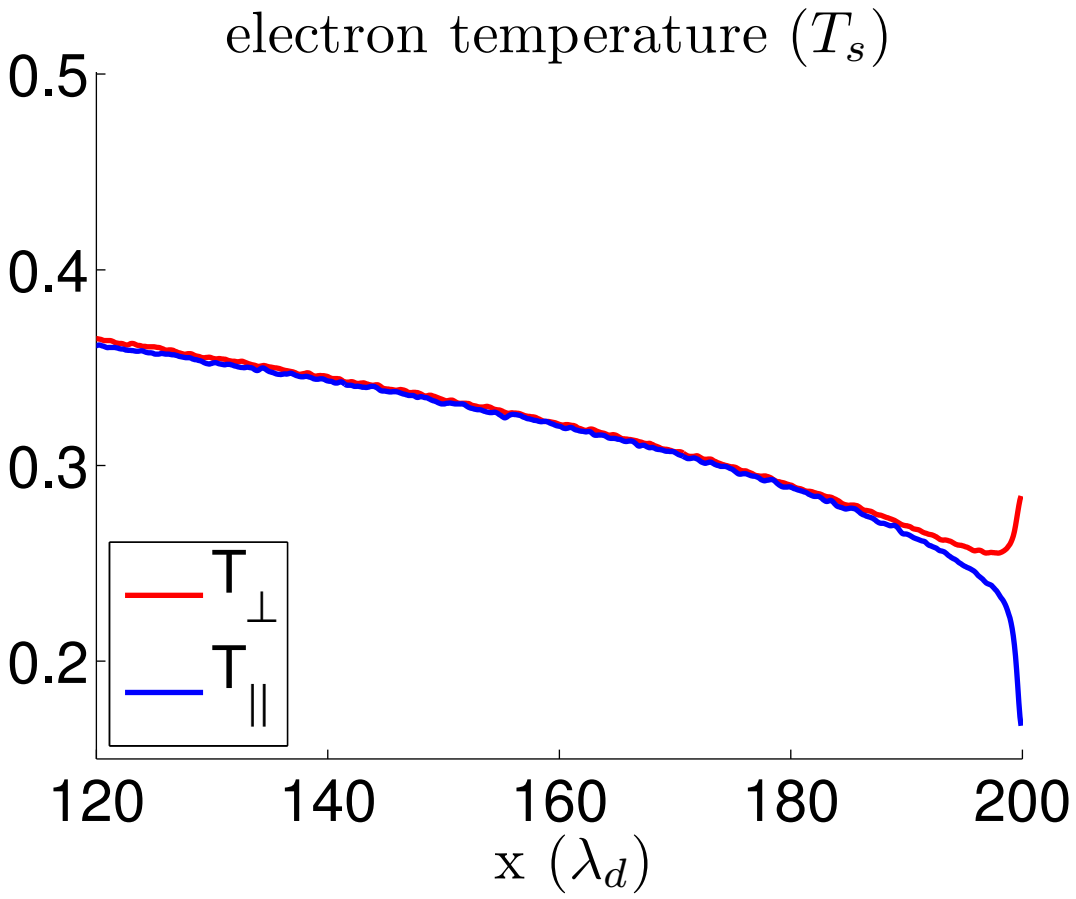
electron temperature (T_s)
0.5
0.4
0.3
0.2
T⊥
T||
120
140
160
180
200
x (λ_d)

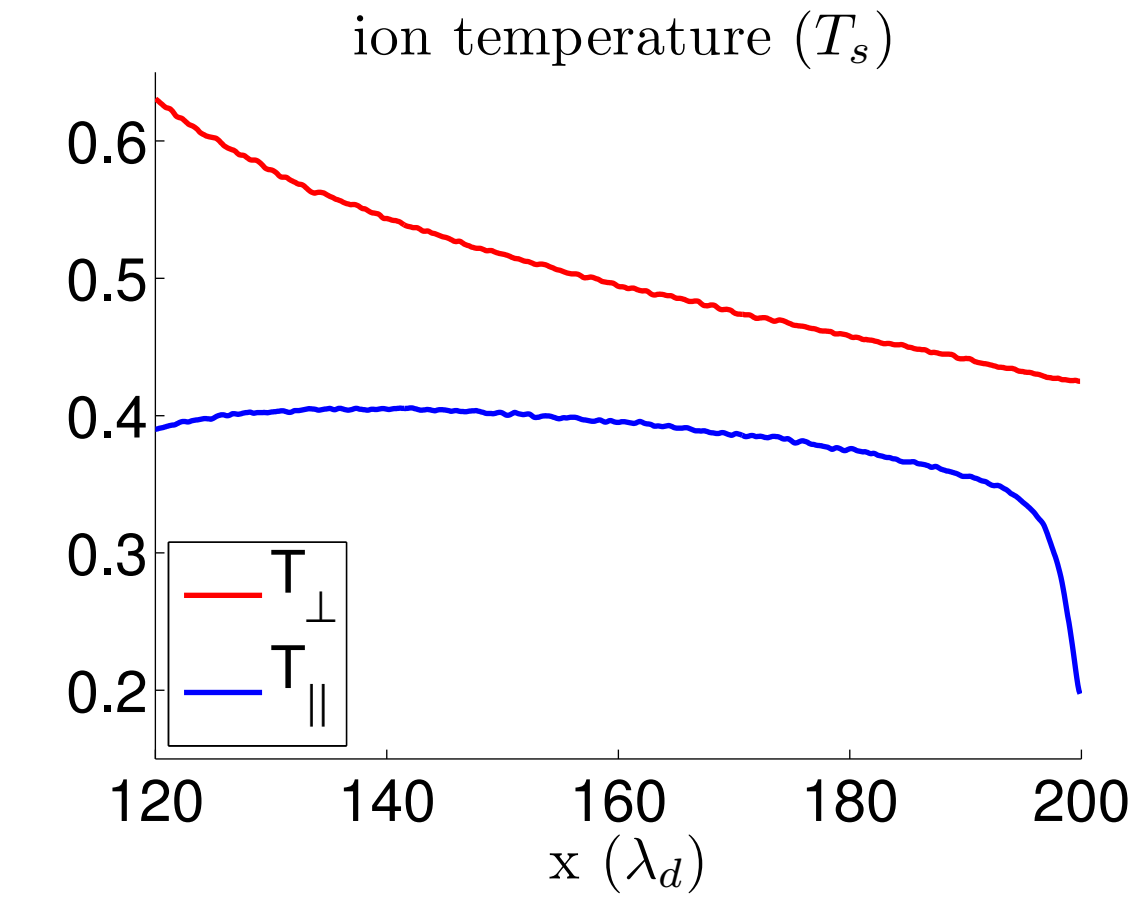
ion temperature (T_s)
0.6
0.5
0.4
0.3
0.2
T⊥
T||
120
140
160
180
200
x (λ_d)

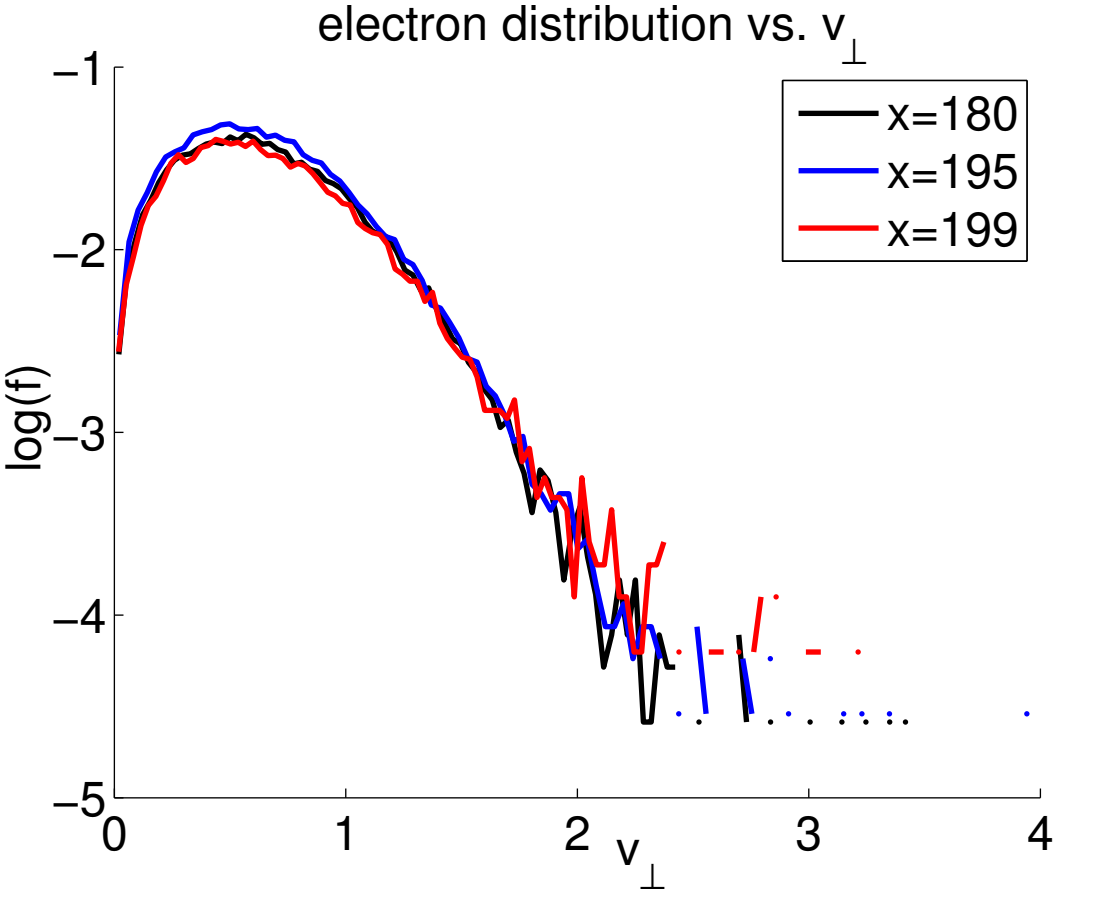
electron distribution vs. v⊥
x=180
x=195
x=199
log(f)
−1
−2
−3
−4
−5
0
1
2
3
4
v⊥

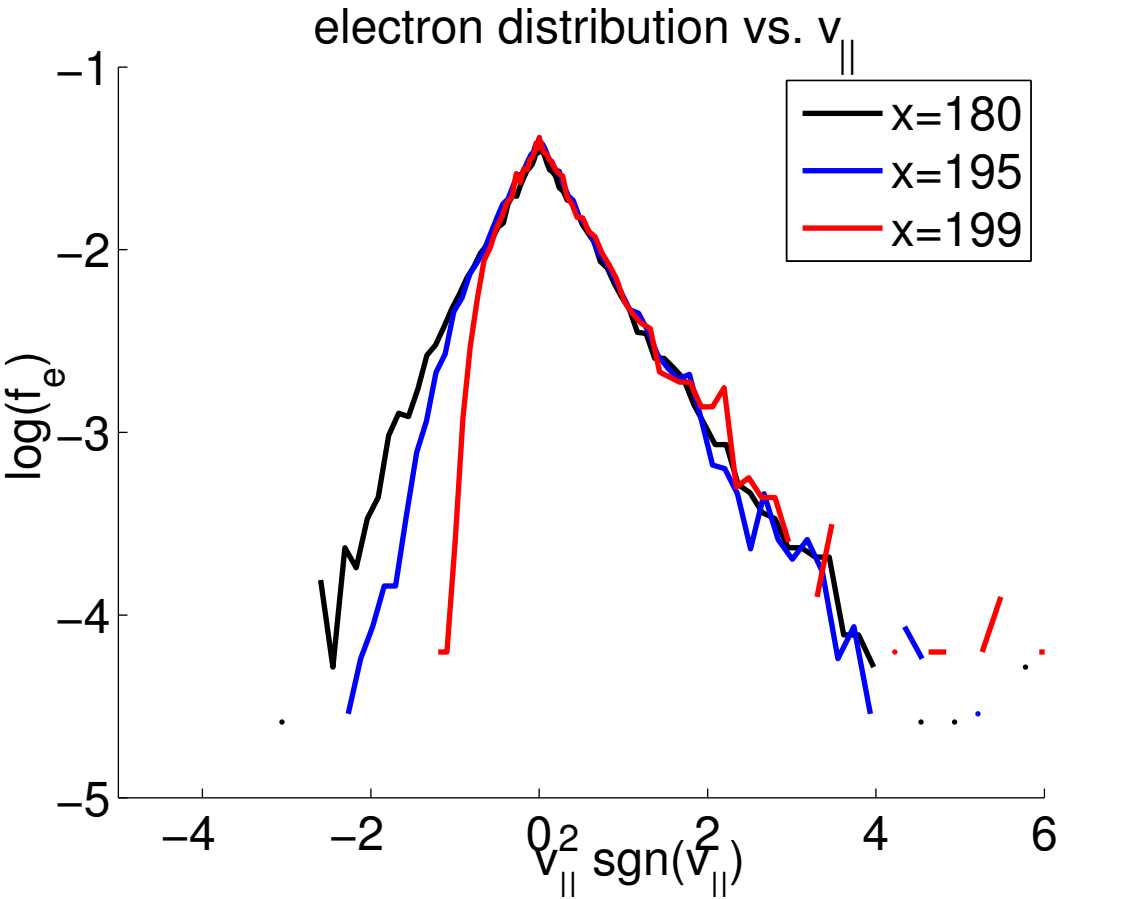
electron distribution vs. v||
x=180
x=195
x=199
log(fe)
−1
−2
−3
−4
−5
−4
−2
0
2
4
6
v||2 sgn(v||)